Application of imaging spectroscopic reflectometry for characterization of gold reduction from organometallic compound by means of plasma jet technology

Jiří Vodák[a,*], David Nečas[b], David Pavliňák [c], Jan M Macak[d], Tomáš Řičica[e] Roman Jambor[e] and Miloslav Ohlídal[a,f]

a) Institute of Physical Engineering, Faculty of Mechanical Engineering, Brno University of Technology, Technická 2, 616 69 Brno, Czech Republic,

b) RG Plasma Technologies, CEITEC Masaryk University, Kamenice 5, 625 00 Brno, Czech Republic

c) Department of Physical Electronics, Masaryk University, Kotlářská 2, 611 37 Brno, Czech Republic

d) Center of Materials and Nanotechnologies, Faculty of Chemical Technology, University of Pardubice, Nám. Čs. Legií 565, 530 02 Pardubice, Czech Republic

e) Department of General and Inorganic Chemistry, Faculty of Chemical Technology, University of Pardubice, Studentská 573, 532 10 Pardubice, Czech Republic

f) Institute of Physics, Faculty of Mining and Geology, VŠB – Technical University of Ostrava, Czech Republic

*) Corresponding author: e-mail: jiri.vodak@yahoo.com

Abstract

This work presents a new application of imaging spectroscopic reflectometry to determine a distribution of metallic gold in a layer of an organogold precursor which was treated by a plasma jet. Gold layers were prepared by spin coating from a solution of the precursor containing a small amount of polyvinylpyrrolidone on a microscopy glass and then they were vacuum dried. A difference between reflectivity of metallic gold and the precursor was utilized by imaging spectroscopic reflectometry to create a map of gold distribution using a newly developed model of the studied sample. The basic principle of the imaging spectroscopic reflectometry is also shown together with the data acquisition principles. XPS measurements and microscopy observations were made to complete the imaging spectroscopic reflectometry results. It is proved that the imaging spectroscopic

reflectometry represents a new method for quantitative evaluation of local reduction of metallic components from metaloorganic compounds.

Both emails are basically the same (they are just two aliases). I (as corresponding author) prefer to use the jiri.vodak@yahoo.com

Keywords: gold reduction, imaging spectroscopic reflectometry, organometallic compound, plasma jet.

1. Introduction

The plasma treatment of noble metal precursors was most recently utilized for deposition of noble metal (including gold) layers by plasma-assisted Atomic Layer Deposition [1,2], but also as a method suitable for the synthesis of metal nanoparticles [3–6] , or in the field of restoration and preservation of metal corrosion [7]. Those applications usually result in layers or surfaces non-uniform in their parameters along their area. If one of these parameters is reflectance, imaging spectroscopic reflectometry (ISR) [1] could be very suitable to quantitatively characterize this non-uniformity.
In this paper we present a brief description of ISR technique and as an illustration of its application potential we deal with a simple example of detection of area distribution of gold in its oxidation state Au^0 (metallic state). The results achieved by the ISR technique are verified by XPS analysis and optical microscopy observations. Three types of samples were prepared for the experimental comparison. The first sample is a reference sample of a gold layer prepared on a glass sheet by magnetron sputtering. The second sample, which was prepared by the spin-coating method, consists of a layer of the polymer and gold in the form of an organogold precursor. In this case, gold is in the oxidation state of Au^{+I}. The third sample was prepared by the same method as the second sample and it was exposed to the plasma discharge. The radiofrequency plasma jet [8] operated in flux of argon was used for reduction of gold cations within the gold precursor to metallic gold. ISR measurements were performed using an imaging spectroscopic reflectometer (ISRM) developed at The Institute of Physical Engineering at Brno University of Technology [9,10].

2. Experimental

2.1. Samples preparation

The organogold(I) precursor $LAu(PPh_3)$, where L is $[o\text{-}C_6H_4(CH{=}NC_6H_3iPr_2\text{-}2,6)]$ ($M = 723\ g.mol^{-1}$) was synthesized by the reaction of parent organolithium derivative LLi with $[AuCl(PPh_3)]$ according to the literature [11]. 2.17 g of the precursor was dissolved in 5 ml of CH_2Cl_2 (Sigma Aldrich) containing a small amount of polyvinylpyrrolidone (0.8 g, K40, Sigma Aldrich) to give solution with c = 0.6 M. The Au layers were prepared by spin coating of as-prepared solution (1 ml per sample) on a microscopy glass using SpinMaster spin coater (Chemat Technology, Inc.) using sequence of two steps – 500 rpm for 1 sec, 10 000 rpm for 30 sec. After spin-coating, the layers were vacuum dried at 125°C using vacuum oven at pressure of 1 mBar. The thickness of the as-dried layers was approximately 6 μm (measured by profilometer Dexta XT, Bruker Corp.).

---

1 **Abbreviations:** ISR – imaging spectroscopic reflectometry; ISRM – imaging spectroscopic reflectometer; VASE – variable angle of incidence spectroscopic ellipsometry; NNSR – near-normal incidence spectroscopic reflectometry;

2.2. Plasma treatment

The scheme of set-up used for the plasma treatment of organogold layers in this work is shown in figure 1(a). An atmospheric plasma jet driven by 13.56 MHz at 180 W was selected as a plasma source [8]. The powered electrode was separated from the plasma by a silica tube with inner diameter of 2 mm and the discharge is ignited in argon (flow rate 5 slm) and admixture of oxygen (flow rate 0.2 slm) flowing through the tube. Distance between the sample and the end of silica tube was set to 15 mm and the treatment time at 30 s. In the next step, the sample surface was imaged by a confocal microscope Olympus LEXT 4000. In figure 1(b) there are clearly visible three different areas, out of which two show a metallic gold appearance. The first area (marked by letter "A") was represented by a circle, and it is an area that appeared directly within the axis of the plasma jet. The second area (marked as "B") was represented by a ring in a distance 3-5 mm from the center of the circle. The third area (marked as "C") was outside the first two areas and it is the farthest area from the intact area of the plasma jet. These areas were then analyzed using an XPS. The ISR measurement was executed in such an area so it will accommodate the three areas.

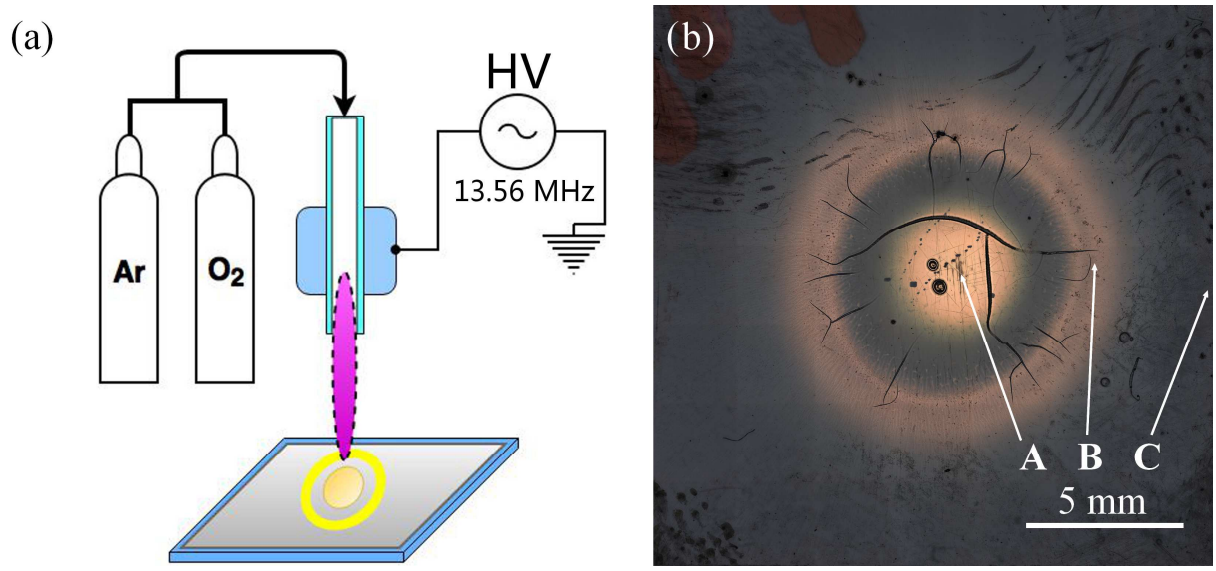

Figure 1: Schematically set-up of plasma treatment (a) and a picture of treated surface (b) Letters show the regions of XPS analysis: A – center, B – ring, C – border. Picture (b) was taken by a confocal microscope.

.

2.3. Imaging spectroscopic reflectometry

ISR developed at aforementioned institute [9,10,12,13] has been mainly used to evaluate local optical parameters (local thickness, spectral dependences of local refractive index and local extinction coefficient) of non-uniform thin films. In certain cases ISR can be used as a standalone technique, but generally it is worthwhile to combine it with conventional (non-imaging) ellipsometric and spectrophotometric techniques (e.g. variable angle of incidence spectroscopic ellipsometry (VASE) and near-normal incidence spectroscopic reflectometry (NNSR)). Using an appropriate dispersion model of optical constants and structural model of a thin film under study the aforementioned combination of techniques can provide (in principle) maps of further interesting thin film parameters like the band gap, maximum energy limit of the transition of electrons interacting with photons and concentration of electrons taking part in the relevant transition [14,15]. In some cases it is possible to determine also a map of thin film boundary roughness [16]. The utilization of ISR, VASE and NNSR combination was shown also promising in the complicated case [17] when the studied film exhibits an inhomogeneity in refractive index along the direction normal to boundaries of the film. The technique of ISR has been used and verified in many cases for optical characterization of thin films [13,15,16,18–20]. Other approaches to ISR technique, different from the approach presented in this

paper, were developed by other groups using different concepts: either combination of imaging and a scanning probe in white light [21,22] or a microscope like device focused on a very high spatial resolution to evaluate electronic devices [23]. Possibilities and limitations of ISR in optical characterization of thin films are transparently presented in the paper [24].

2.3.1. Imaging spectroscopic reflectometer

The set-up of the ISRM we used is presented in figure 2:

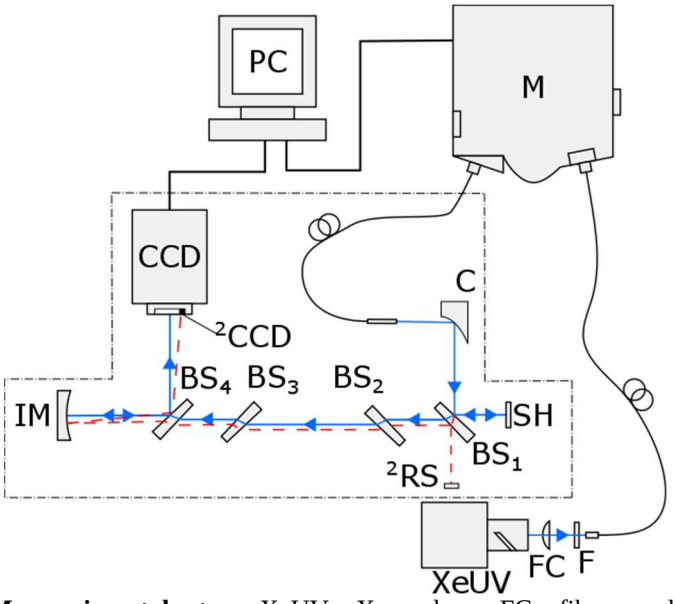

Figure 2: **The ISRM experimental set-up**; XeUV – Xe arc lamp, FC – fiber coupler, F – filter, M – monochromator, C – collimator, BS_{1-4} – beamsplitters and wedge compensators, SH – sample holder, ^{2}RS - 2nd channel reference sample, IM – imaging mirror, CCD – CCD camera, ^{2}CCD – part of the CCD chip used as a the second channel detector, PC – personal computer.

A source of light for the ISRM is a XeUV broad light spectra arc lamp. Single wavelengths are selected from the spectra by the computer-controlled monochromator. The lamp, the monochromator and the ISRM itself are connected by two identical UV capable optical fibers. The off axis parabolic mirror C with the optical fiber output situated at the focal point of the mirror creates a collimated monochromatic light beam which illuminates (by reflection on the beamsplitter BS_1) perpendicularly a sample in the sample holder SH (it can be assumed that the angle of incidence along the whole sample surface is identical). The sample reflects the light directly back. The reflected light goes through the system of four fused silica wedges BS_1 – BS_4 (BS_1 is the aforementioned beamsplitter and it has a beam splitting layer) to a simple spherical mirror IM. This mirror then creates an image of the sample surface on a chip of the CCD camera which records the image. The four-wedge system corrects optical dispersion and removes secondary reflections of the beamsplitter BS_1. The wedge BS_4 also has a beam splitting layer. This wedge allows in axis imaging. The large collimating mirror C ensures good uniformity of the light beam along its cross-section and it also allows utilization of a small part of the measuring camera chip as a reference channel (further called the 2nd channel) of the ISRM. This is done using the light which passes through the first beamsplitter BS_1 and therefore it is not reflected onto the sample. By positioning a reference sample (further called the 2nd channel sample) in such a way that it will be imaged onto a corner of the chip of the CCD camera, it is possible to obtain information on changes of the light source intensity and subsequently eliminate them (see below). This 2nd channel sample stays in its exact position during all measurements. As it will be described in the next paragraph, measurements with the ISRM are relative, i.e. a measured sample is compared to a reference sample with known reflectivity to eliminate unwanted influence of the optical system of the

ISRM. Maximum size of samples which can be measured by the ISRM, is about 20 mm x 20 mm with the spatial resolution on a sample of 9 lp/mm (single line thickness 56 μm) within the spectral range 270 nm to 1000 nm.

2.3.2. ISR data acquisition

The output experimental data obtained by means of the ISRM, spectral dependencies of local relative reflectivity $R_r^{k,u}(\lambda_n)$ of a studied sample in the form of a matrix $(k,u)^{th}$ element of which corresponds to the $(k,u)^{th}$ small region of the sample. λ_n are values of the light wavelength selected from the whole accessible spectral range with a chosen sampling step, $k = 1…P$; $u = 1...Q$ are coordinates of single pixels, where P and Q are numbers of the CCD camera chip pixels in horizontal and vertical direction. The continuous map of these areas constitutes the investigated sample surface which is imaged by the imaging system of the ISRM on the CCD camera chip.

These signal values are processed in the way corresponding to the two-channel ISRM. This procedure takes into account that the pixel signal value is influenced not only by the corresponding local reflectivity of the sample area, but also by a background signal (for $(k,u)^{th}$ pixel):

$$B^{k,u}(\lambda_n, t_3) = D^{k,u}(\lambda_n) + b^{k,u} I_o(\lambda_n, t_3), \quad (1)$$

where $D^{k,u}(\lambda_v,t_3)$ is the background signal generated by camera electronics (dark current, camera bias, readout and amplifier noises etc.), $I_o(\lambda_n,t_3)$ is the light source intensity, $b^{k,u}$ is a constant of proportionality, $b^{k,u}I_o(\lambda_v,t_3)$ is the background light scattered inside of the apparatus and t_3 is the time of $D^{k,u}I_o(\lambda_v,t_3)$ record. Camera electronics noise $D^{k,u}$ can be eliminated by subtracting dark images (images made with the camera shutter closed, with the exposure time equals the exposure time of the corresponding signal image). This is done immediately after the image signal acquisition. Therefore $D^{k,u}$ is not considered further.

The signal processing procedure consists of three steps:

- the first step – measurement of a reference sample,
- the second step – measurement of a studied sample,
- the third step – measurement of the signal originating from the background light scattered inside the ISRM.

The signal, acquired from a $(k,u)^{th}$ CCD camera pixel, is now written (with the background and already without the $D^{k,u}$ term) as follows:

$$S_{J,i}^{k,u}(\lambda_n, t_i) = I_o(\lambda, t_i)\left[\eta^{k,u}(\lambda) R_i^{k,u}(\lambda_n) + b^{k,u}\right], \quad (2)$$

where index $J = m$ for “measuring channel” and $J = s$ for “second channel”, index $i = 1$ for the reference sample, $i = 2$ for the studied sample and $i = 3$ for measurement of the background (without any sample), $I_0(\lambda_n,t_i)$ is the intensity of the monochromatic light from the monochromator, $\eta^{k,u}(\lambda_n)$ is the apparatus function (it describes the influence of the apparatus – optic elements, quantum efficiency of the camera, amplification of the signal etc.). $R_i^{k,u}(\lambda_n, t_i)$ is the local absolute reflectivity of the current sample depending on the index value. Because for index $i = 3$ the reflectivity is equal to 0 (no sample in the holder), the first part of the formula (2) is then also equal to 0 and only the background

$b^{k,u}I_o(\lambda_v,t_3)$ remains. The following formula (3) ensures elimination of a possible time non-stability of the light source of the ISRM (i.e. $I_0(\lambda_n,t)$) and the influence of the background:

$$R_r^{k,u}(\lambda) = \frac{\frac{S_{m,2}^{k,u}(\lambda,t_2)}{S_{s,2}(\lambda,t_1)} - \frac{S_{m,3}^{k,u}(\lambda,t_3)}{S_{s,3}(\lambda,t_2)}}{\frac{S_{m,1}^{k,u}(\lambda,t_1)}{S_{s,1}(\lambda,t_0)} - \frac{S_{m,3}^{k,u}(\lambda,t_3)}{S_{s,3}(\lambda,t_2)}} = \frac{R_2^{k,u}(\lambda)}{R_1^{k,u}(\lambda)}, \quad (3)$$

where $R_r^{k,u}(\lambda_n)$is the sought spectral dependence of the local relative reflectivity of the studied sample of an area which is imaged onto the $(k,u)^{th}$ CCD pixel. It is possible to determine interesting parameters of studied samples from the map of these local relative reflectivity spectral dependencies. Exactly these dependencies are used for quantitative localization of areas with metallic gold reduced from organometallic compound by means of a plasma jet technology. According to the best of our knowledge this is the first application of the ISR in such a task.

2.3.3. ISR data analysis

Because the samples studied in this work differ considerably from the samples characterized by ISR in previous studies [13,15,16,18,19], it was necessary to develop a new data analysis procedure. In those previous studies, mapping the thin film thickness in each pixel was always among the primary goals and interference in the reflectance spectra were utilized. In the presented case, the layers were relatively thick (approx. 6 μm), non-uniform and their refractive index of the organic material was similar to that of the glass substrate. Therefore, in parts where they were transparent, only slight interference in the layer was observable. In parts where gold was reduced by plasma discharge, the layers were of course non-transparent. The layers were thus modelled as thick slabs, disregarding interference completely.

Considering the description of interaction of light with an organic slab containing partially reduced gold, a number of possible models are imaginable. Two basic approaches correspond to the assumptions that the domains formed by each material are either much smaller than the light wavelength or much larger. In the first approach the material was modelled as a mixture of the organic material and gold using an effective medium approximation formula [25]. In the second approach it was possible to assume that a part of the incident light was reflected from one material and part from the other. The reflectivity was thus calculated by weighted averaging of reflectivity of the two materials. Beside these two basic approaches it was of course possible to consider more complex models including refractive index profiles, scattering or additional intermediate materials. However, the huge quantity of ISR data dictates the utilization of a relatively simple model. Furthermore, as the layers were quite far from ideal ones the reflectivity spectra exhibited various defects and distortions. A robust model extracting useful information even from relatively poor quality spectra was thus required.

Either of the two basic models was suitable from this point of view. Both also have another useful property. When the optical constants of the two materials are fixed, both models are described using a single parameter representing the relative amount of each material. This parameter can be chosen for instance as the gold fraction. It must be nevertheless emphasized that the meaning of such a parameter is different in each of the two models. For the mixing model the parameter describes the volume fraction of gold, whereas in the separated model the parameter describes the area fraction of gold. Choice between the models is essentially determined by the fact, which of them fits the experimental data better. The two models considered were:

- thick slab with optical constants described by either the Maxwell-Garnett or Bruggeman formula (mixing),
- thick slab with areas covered by the organic compound and metallic gold (separated).

Of these two the second (separated) model agreed with the experimental data better, both quantitatively by resulting in smaller residual sums of squares and qualitatively. In particular in the long-wavelength region it was the only model whose general behavior matched experimental spectra. Hence, this last model was further used in this work. Nevertheless, it should be noted that gold fractions obtained using the two types of models were highly correlated.
The parameter p which enables us to quantify the distribution of reduced gold is defined as follows:

$$p^{k,u} = \frac{A_{gold}^{k,u}}{A_{reg}^{k,u}} \quad (4)$$

where $A_{gold}^{k,u}$ is the area which metallic gold fills in the region of the sample corresponding to the $(k,u)^{th}$ CCD camera pixel and $A_{reg}^{k,u}$ is the area of this whole region.
Then the resulting measured local relative reflectivity of the studied sample (organogold precursor treated by plasma jet) region corresponding to the (k,u)th CCD camera pixel is

$$R^{k,u}(\lambda_n) = p^{k,u}R_{gold}(\lambda_n) + \left(1 - p^{k,u}\right)R_{org}(\lambda_n,) \quad (5)$$

where $R_{gold}(\lambda_n)$ is the spectral dependence of relative reflectivity of gold obtained by measuring the first reference sample of a gold layer prepared on a glass sheet by magnetron sputtering. $R_{org}(\lambda_n)$ is the spectral dependence of relative reflectivity of the organogold precursor layer (the second sample type, which was not treated by plasma jet). It was assumed that both of last mentioned samples can be considered as uniform in reflectivity. The map of $p^{k,u}$ and thus the map of metallic gold distribution reduced from the organogold precursor by plasma jet thermal treatment was determined by least squares method using the equation (5).

2.4. Photoelectron X-ray spectroscopy

The XPS measurements were performed using ESCALAB 250Xi (ThermoFischer Scientific) equipped with 500 mm Rowland circle monochromator with focused Al Kα X-ray source (200 W power, 650 μm spot size). Data acquisition and processing were carried out using CasaXPS software, version 2.3.15 (Casa Software Ltd., UK). The binding energy (BE) scale was corrected for charging using an electron BE of 284.8 eV for the aliphatic carbon component of survey spectra. Hi-res spectra of gold were fitted into six contributions in three oxidation states. According to literature [26,27], the peaks of metal gold Au^0 were assigned to BE = 83.7 eV (4f 7/2) and BE = 87.3 eV (4f 5/2). The gold contributions in oxidation state Au^{+I} were fitted with 85.3 eV (4f 7/2) and 88.9 eV (4f 5/2). Binding energy of gold in oxidation state Au^{+III} was assigned to 86.4 eV (4f 7/2) and 90.0 eV (4f 5/2). The full width at half maximum of all Au 4f components was in the range 0.8-1.4 eV.

3. Results and discussion

3.1. ISR results

Data obtained as described in paragraph 2.3.2 and analyzed according to paragraph 2.3.3 are shown in figure 3. This figure shows a quantitative area distribution of metallic gold reduced by plasma jet thermal treatment of the organogold precursor. The map is colored according to the value of the parameter *p*. Black areas are cracks in the layer which occurred after the heat treatment. Letters A,B and C denote the same three spots measured by XPS as marked in figure 1(b).

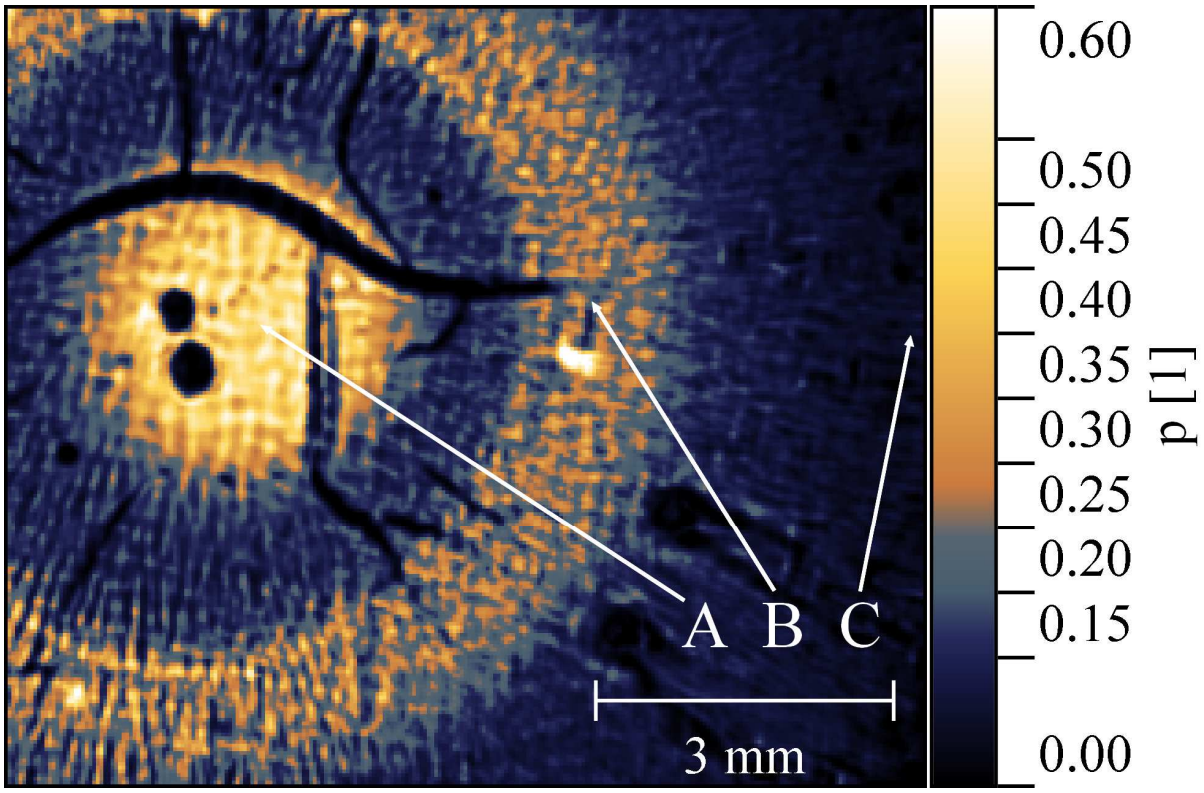

Figure 3: **Figure 3: A metallic gold map obtained by ISR measurements**. The scale shows a value of the model parameter p– the area fraction of metallic gold in the organogold precursor treated by plasma jet.

For a comparison with the XPS results, spectral dependencies of local relative reflectivity of the three spots selected from the ISR measurement data are shown in figure 4. To complete the figure, it also contains spectral dependencies of relative reflectivity of a pure gold layer and also of relative reflectivity of the organogold layer without any plasma jet thermal treatment.
It can be clearly seen how the amount of metallic gold influences the local relative reflectivity of the studied sample along its area. The center A contains most metallic gold, the ring B contains less, but still a significant amount of gold, while the outer area C is basically untreated and thus without metallic gold.

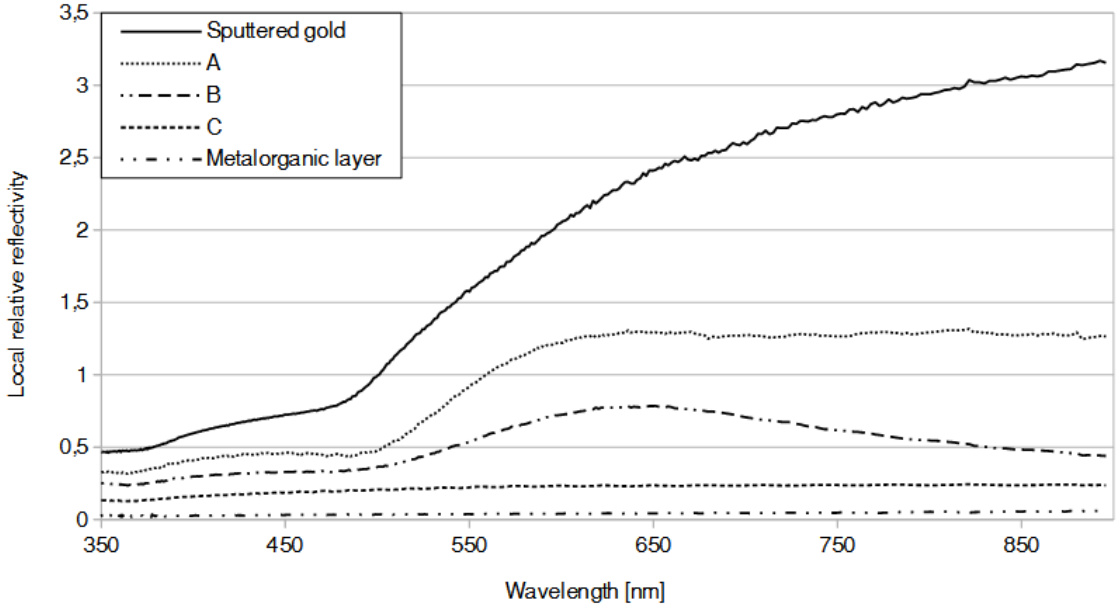

Figure 4: Reflectivity comparison. Measured relative reflectivity of the spots (marked in figures 1(b) and 3) on the measured sample together with measurements of pure gold layer and the organogold layer without any plasma jet treatment.

3.2. XPS results

Results of elemental analysis of gold layers are shown in table 1. Surprisingly, the 30 nm thick Au sputtered layer shows a relative high content of carbon on the sample surface. From the literature, we can learn that this is a common phenomenon. The only way to prepare and characterize the metal layers in a very pure state is their preparation, transport and measuring all time in the high vacuum – preferably in-line in XPS [26]. A sample with the spin-coated organic gold-precursor has a relatively small content of gold, as expected a high percentage of carbon will come from used carrier polymer (PVP) and precursor decomposition residues. After the plasma treatment, a significant increase of gold and oxygen content was observed in the areas of the center (A) and the ring around the center (B). As well as an increase of Au and O, the decrease of carbon was detected, which shows the oxidation processes of the carrier polymer. Both processes are probably related to the degradation of the organic precursor, and to the continuing reduction and concentration increase of metal gold.

		Elemental analysis (at. %)					**Concentration (at.%)**		
Samples		**Au 4f**	**O 1s**	**C 1s**	**P 2p**	**N 1s**	**Au^0**	**Au^{+I}**	**Au^{+III}**
Metal gold		67.7	1.9	30.4	-	-	95.9	4.0	0.0
Gold precursor		2.8	3.8	88.6	3.2	1.6	6.7	87.4	5.9
	A – center	4.9	51.8	40.2	3.2	-	91.1	8.8	0.1
Plasma	**B – ring**	11.9	40.4	43.1	4.6	-	93.1	5.8	1.0
treated	**C – border**	0.5	8.9	89.7	0.8	-	-	-	-

Table 1: Elemental compositions of gold layer sputtered on glass slide, initial organic-gold precursor and the sample treated in plasma discharge by deconvolution of XPS spectra of Au 4f hi-res peaks.

Figure 5 shows the highly resolved XPS Au 4f spectra of the coated gold layer, the non-treated gold precursor and the plasma treated sample in the area of center (A in fig. 3) and the ring (B in fig. 3). The hi-res Au 4f spectrum of the sample border (C in fig. 3) is not presented due to the low signal/noise ratio reflecting the low concentration of gold. However, the spectrum of the region (C in fig. 3) was similar to the spectrum of the gold precursor. The data in table 1 show the distribution of the oxidation states in the samples. Metallic gold (figure 5(b)), which is characteristic by the oxidation state Au^0, is present in the sample of 30 nm coated Au layer, according to expectations. As it was confirmed, the organic precursor (figure 5(a)) contains gold primarily in the oxidation state Au^{+I}. The samples treated by the plasma discharge (figure 5(c), (d)) show the significant reduction of the oxidation state of gold from Au^{+I} to Au^0. Finally, into the fitting model was added the oxidation state Au^{+III} (e.g. typically in Au_2O_3), this contribution, however, plays a minor role.

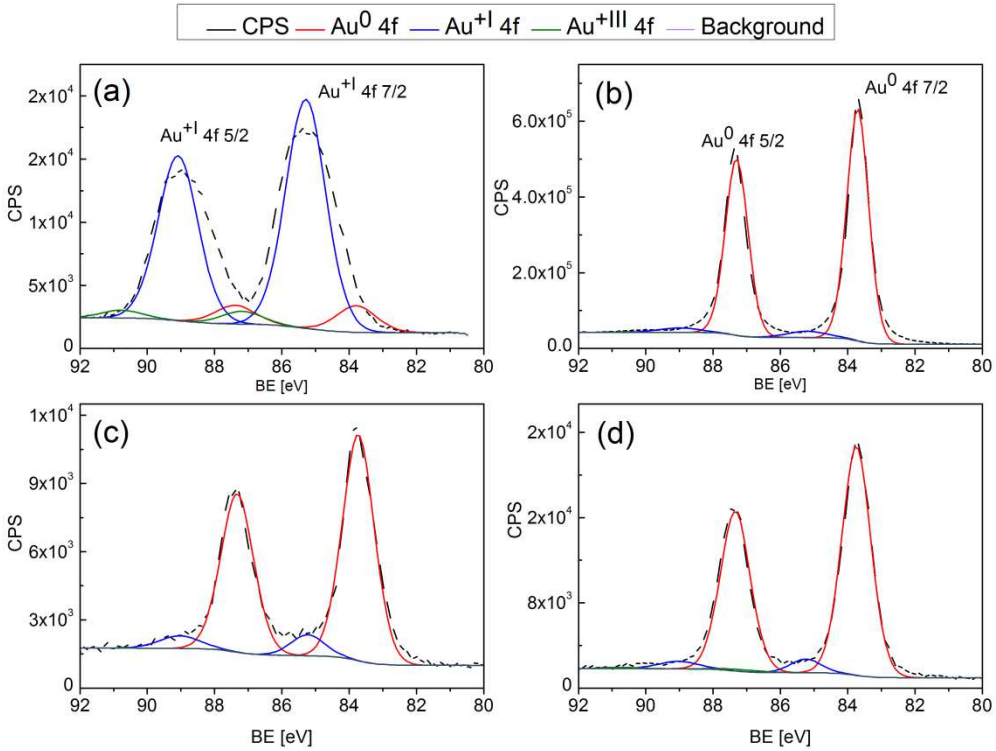

Figure 5: XPS Au 4f hi-res spectra of the samples measured. Organic gold precursor (a), coated gold layer (b), plasma treated sample in the center (c) and in the ring (d).

3.3. Comparison of the techniques

Figures 3 and 4 show that ISR technique is capable of evaluating a sample with plasma reduced metallic gold. Imaging nature of the ISR technique is ideal for such non uniform sample. It can be seen that metallic gold was mostly reduced around the point where plasma jet was applied, but also formed a ring around the central spot. While the confocal microscope picture (figure 1(b)) looks better than the map obtained from ISR thanks to its higher resolution, it does not provide quantitative information. In contrast, ISR data can be used to quantify the relative amount of metallic gold or at least obtain semi-quantitative information. The accuracy depends on the layer quality and its chosen model. If we compare the values in the map in figure 3 with gold concentrations from XPS analysis in table 1, it is immediately evident that the metallic gold fractions determined by ISR are much higher. The reason is that the two techniques measure different quantities. XPS is a surface sensitive technique that measures the composition of top several nanometers of the layer, whereas ISR determines gold coverage regardless of how deep gold is embedded in the layer. It should be also noted that the lower

resolution is not an inherent limitation of ISR as it is only given by the construction of the particular device used here. It can be improved [28].

4. Conclusion

The ISR represents a new method to quantitatively evaluate local reduction of metallic components from metaloorganic compounds, as shown on a model example of organogold precursor. Its imaging nature allows evaluating large areas of samples at once as it was shown. A map of metallic gold can be obtained from the measurement data. The measurement of local relative reflectivity along larger areas of surfaces can be used in various ways. While usually the aim of the measurement are the optical constants of a material, specific reflectivity of metals can be used to identify them and create maps of the material along the surface. This can be useful as it was presented here especially when analyzing organometallic compounds and their plasma treatment. Combination with other measurement techniques might also be possible to obtain measurements with even higher accuracy – similarly as ISR technique is used in combination with VASE and NNSR for evaluation of local optical constants and local thickness of non-uniform thin film samples along their surface.

Acknowledgements:

We thank Dr. Jiří Černý (COC Ltd., Rybitví) for profilometric measurements.

Funding: This work was supported by the Technology Agency of Czech Republic [grant numbers TA02010784, TE01020022]; the Brno University of Technology specific research fund [grant number FSI-S-14-2494]; the Ministry of Education, Youth and Sports of the Czech Republic [project numbers LO1411, LQ1601]; the European Regional Development Fund [project number CZ.1.05/2.1.00/03.0086]; and the Czech Science Foundation [project number 15-07912S].

References

[1] H.B. Profijt, S.E. Potts, M.C.M. van de Sanden, W.M.M. Kessels, Plasma-Assisted Atomic Layer Deposition: Basics, Opportunities, and Challenges, J. Vac. Sci. Technol. A. 29 (2011) 50801. doi:10.1116/1.3609974.

[2] M.B.E. Griffiths, P.J. Pallister, D.J. Mandia, S.T. Barry, Atomic Layer Deposition of Gold Metal, Chem. Mater. 28 (2015) 44–46. doi:10.1021/acs.chemmater.5b04562.

[3] J.-J. Zou, Y. Zhang, C.-J. Liu, Reduction of Supported Noble-Metal Ions Using Glow Discharge Plasma, Langmuir. 22 (2006) 11388–11394. doi:10.1021/la061795b.

[4] C. Richmonds, R.M. Sankaran, Plasma-liquid electrochemistry: Rapid synthesis of colloidal metal nanoparticles by microplasma reduction of aqueous cations, Appl. Phys. Lett. 93 (2008) 131501. doi:10.1063/1.2988283.

[5] Z. Wei, C. Liu, Synthesis of monodisperse gold nanoparticles in ionic liquid by applying room temperature plasma, Mater. Lett. 65 (2011) 353–355. doi:10.1016/j.matlet.2010.10.030.

[6] J. Hieda, N. Saito, O. Takai, Exotic shapes of gold nanoparticles synthesized using plasma in aqueous solution, J. Vac. Sci. Technol. A. 26 (2008) 854–856. doi:10.1116/1.2919139.

[7] K. Schmidt-Ott, Plasma reduction: its potential for use in the conservation of metals, in: Proc. Int. Conf. Met. Conserv., National Museum of Australia, Canberra, Australia, 2004.

[8] J. Voráč, P. Dvořák, V. Procházka, J. Ehlbeck, S. Reuter, Measurement of hydroxyl radical (OH) concentration in an argon RF plasma jet by laser-induced fluorescence, Plasma Sources Sci. Technol. 22 (2013) 25016. doi:10.1088/0963-0252/22/2/025016.

[9] M. Ohlídal, I. Ohlídal, D. Franta, T. Králík, M. Jákl, M. Eliáš, Optical characterization of thin films non-uniform in thickness by a multiple-wavelength reflectance method, Surf. Interface Anal. 34 (2002) 660–663. doi:10.1002/sia.1382.

[10] I. Ohlídal, M. Ohlídal, P. Klapetek, V. Čudek, M. Jákl, Characterization of thin films nonuniform in optical parameters by spectroscopic digital reflectometry, in: Wave-Opt. Syst. Eng. II, 2004: pp. 260–271. doi:10.1117/12.509628.

[11] M. Hejda, L. Dostál, R. Jambor, A. Růžička, R. Jirásko, J. Holeček, Synthesis, Structure and Transmetalation Activity of Various C,Y-Chelated Organogold(I) Compounds, Eur. J. Inorg. Chem. 2012 (2012) 2578–02587. doi:10.1002/ejic.201200152.
[12] M. Ohlídal, I. Ohlídal, P. Klapetek, M. Jákl, V. Čudek, M. Eliáš, New Method for the Complete Optical Analysis of Thin Films Nonuniform in Optical Parameters, Jpn. J. Appl. Phys. 42 (2003) 4760–4763. doi:10.1143/JJAP.42.4760.
[13] D. Nečas, V. Čudek, J. Vodák, M. Ohlídal, P. Klapetek, J. Benedikt, K. Rügner, L. Zajíčková, Mapping of properties of thin plasma jet films using imaging spectroscopic reflectometry, Meas. Sci. Technol. 25 (2014) 115201. doi:10.1088/0957-0233/25/11/115201.
[14] D. Franta, D. Necas, L. Zajícková, Models of dielectric response in disordered solids, Opt. Express. 15 (2007) 16230–16244.
[15] M. Ohlídal, I. Ohlídal, P. Klapetek, D. Nečas, A. Majumdar, Measurement of the thickness distribution and optical constants of non-uniform thin films, Meas. Sci. Technol. 22 (2011) 85104. doi:10.1088/0957-0233/22/8/085104.
[16] D. Nečas, I. Ohlídal, D. Franta, M. Ohlídal, V. Čudek, J. Vodák, Measurement of thickness distribution, optical constants, and roughness parameters of rough nonuniform ZnSe thin films, Appl. Opt. 53 (2014) 5606–5614.
[17] D. Franta, I. Ohlídal, P. Klapetek, P. Pokorný, M. Ohlídal, Analysis of inhomogeneous thin films of ZrO2 by the combined optical method and atomic force microscopy, Surf. Interface Anal. 32 (2001) 91–94. doi:10.1002/sia.1013.
[18] I. Ohlídal, M. Ohlídal, D. Nečas, D. Franta, V. Buršíková, Optical characterisation of SiOxCyHz thin films non-uniform in thickness using spectroscopic ellipsometry, spectroscopic reflectometry and spectroscopic imaging reflectometry, Thin Solid Films. 519 (2011) 2874–2876. doi:10.1016/j.tsf.2010.12.069.
[19] D. Nečas, J. Vodák, I. Ohlídal, M. Ohlídal, A. Majumdar, L. Zajíčková, Simultaneous determination of dispersion model parameters and local thickness of thin films by imaging spectrophotometry, Appl. Surf. Sci. 350 (2015) 149–155. doi:10.1016/j.apsusc.2015.01.093.
[20] D. Nečas, I. Ohlídal, D. Franta, V. Čudek, M. Ohlídal, J. Vodák, L. Sládková, L. Zajíčková, M. Eliáš, F. Vižďa, Assessment of non-uniform thin films using spectroscopic ellipsometry and imaging spectroscopic reflectometry, Thin Solid Films. 571, Part 3 (2014) 573–578. doi:10.1016/j.tsf.2013.12.036.
[21] J. Spousta, M. Urbánek, R. Chmelík, J. Jiruše, J. Zlámal, K. Navrátil, A. Nebojsa, T. Šikola, In situ measurements of surface homogeneity of optical parameters of weakly absorbing thin films, Surf. Interface Anal. 34 (2002) 664–667. doi:10.1002/sia.1383.
[22] M. Urbánek, J. Spousta, K. Navrátil, R. Szotkowski, R. Chmelík, M. Buček, T. Šikola, Instrument for thin film diagnostics by UV spectroscopic reflectometry, Surf. Interface Anal. 36 (2004) 1102–1105. doi:10.1002/sia.1850.
[23] K. Kim, S. Kim, S. Kwon, H.J. Pahk, Volumetric thin film thickness measurement using spectroscopic imaging reflectometer and compensation of reflectance modeling error, Int. J. Precis. Eng. Manuf. 15 (2014) 1817–1822. doi:10.1007/s12541-014-0534-3.
[24] M. Ohlídal, I. Ohlidal, D. Nečas, J. Vodák, D. Franta, P. Nádaský, F. Vižd'a, Possibilities and limitations of imaging spectroscopic reflectometry in optical characterization of thin films, in: A. Duparré, R. Geyl (Eds.), 2015: p. 96280R. doi:10.1117/12.2191052.
[25] X.C. Zeng, D.J. Bergman, P.M. Hui, D. Stroud, Effective-medium theory for weakly nonlinear composites, Phys. Rev. B. 38 (1988) 10970–10973. doi:10.1103/PhysRevB.38.10970.
[26] J.F. Moulder, W.F. Stickle, P.E. Sobol, K.D. Bomben, Handbook of X-ray photoelectron spectroscopy: a reference book of standard spectra for identification and interpretation of XPS data, ULVAC-PHI, Inc, Enzo, Japan, 1995.
[27] B. Vincent Crist, Handbook of Monochromatic XPS Spectra: The Elements of Native Oxides, 2000.
[28] J. Vodák, V. Čudek, P. Nádaský, M. Ohlídal, Imaging spectroscopic reflectometer based on pellicle beamsplitter, in: Proc. SPIE 9626, Jena, Germany, 2015: p. 96262L–8. doi:10.1117/12.2190947.